PNAS RESEARCH ARTICLE | GENETICS

Deficiency of the minor spliceosome component U4atac snRNA secondarily results in ciliary defects in human and zebrafish

Deepak Khatri[a,1], Audrey Putoux[a,b,1], Audric Cologne[a,c], Sophie Kaltenbach[d], Alicia Besson[a], Eloïse Bertiaux[e], Justine Guguin[a], Adèle Fendler[a], Marie A. Dupont[f], Clara Benoit-Pilven[a,c], Leila Qebibo[g], Samira Ahmed-Elie[g], Séverine Audebert-Bellanger[h], Pierre Blanc[i], Thomas Rambaud[i], Martin Castelle[j], Gaëlle Cornen[k], Sarah Grotto[l], Agnès Guët[m], Laurent Guibaud[n], Caroline Michot[o,p], Sylvie Odent[q], Lyse Ruaud[r,s], Elise Sacaze[t], Virginie Hamel[e], Rémy Bordonné[u], Anne-Louise Leutenegger[r], Patrick Edery[a,b], Lydie Burglen[g,p], Tania Attié-Bitach[d,p], Sylvie Mazoyer[a,1], and Marion Delous[a,1,2]

Edited by Christine Seidman, Harvard Medical School, Boston, MA; received February 12, 2021; accepted December 12, 2022

In the human genome, about 750 genes contain one intron excised by the minor spliceosome. This spliceosome comprises its own set of snRNAs, among which U4atac. Its noncoding gene, *RNU4ATAC*, has been found mutated in Taybi-Linder (TALS/microcephalic osteodysplastic primordial dwarfism type 1), Roifman (RFMN), and Lowry-Wood (LWS) syndromes. These rare developmental disorders, whose physiopathological mechanisms remain unsolved, associate ante- and post-natal growth retardation, microcephaly, skeletal dysplasia, intellectual disability, retinal dystrophy, and immunodeficiency. Here, we report bi-allelic *RNU4ATAC* mutations in five patients presenting with traits suggestive of the Joubert syndrome (JBTS), a well-characterized ciliopathy. These patients also present with traits typical of TALS/RFMN/LWS, thus widening the clinical spectrum of *RNU4ATAC*-associated disorders and indicating ciliary dysfunction as a mechanism downstream of minor splicing defects. Intriguingly, all five patients carry the n.16G>A mutation, in the Stem II domain, either at the homozygous or compound heterozygous state. A gene ontology term enrichment analysis on minor intron-containing genes reveals that the cilium assembly process is over-represented, with no less than 86 cilium-related genes containing at least one minor intron, among which there are 23 ciliopathy-related genes. The link between *RNU4ATAC* mutations and ciliopathy traits is supported by alterations of primary cilium function in TALS and JBTS-like patient fibroblasts, as well as by *u4atac* zebrafish model, which exhibits ciliopathy-related phenotypes and ciliary defects. These phenotypes could be rescued by WT but not by pathogenic variants-carrying human U4atac. Altogether, our data indicate that alteration of cilium biogenesis is part of the physiopathological mechanisms of TALS/RFMN/LWS, secondarily to defects of minor intron splicing.

genetic disease | splicing | minor introns | U4atac | primary cilium

Pathogenic variants of the noncoding *RNU4ATAC* gene, transcribed into the U4atac small nuclear RNA (snRNA) involved in minor splicing, are associated with three rare autosomal recessive syndromes: Taybi-Linder (TALS, also named microcephalic osteodysplastic primordial dwarfism type 1) (1, 2), Roifman (RFMN) (3), and Lowry-Wood (LWS) (4) syndromes. TALS, RFMN, and LWS patients are characterized by distinct patterns of skeletal dysplasia and different degrees of severity of ante- and post-natal growth retardation, microcephaly, intellectual disability, retinal dystrophy, and immunodeficiency, as well as variable accompanying traits including syndrome-specific facial dysmorphism, dermatitis, hepatomegaly (RFMN), endocrine abnormalities, and reduced survival (TALS) (5, 6). TALS patients also display severe cerebral malformations including abnormal gyral pattern, corpus callosum abnormalities, and hypoplasia of cerebellar vermis. For those who carry a specific recurrent *RNU4ATAC* mutation (n.51G>A), death usually occurs within the first two years of life, rapidly after an apparently trivial infectious episode, for yet unknown reasons.

The U4atac snRNA is a component of the minor spliceosome involved in the splicing of the so-called minor or U12-type introns recognized through their consensus splice site sequences (7). Their number is highly variable depending on the species (8); according to an up-to-date analysis of the GRCh38 genome assembly, there are 850 of them scattered in 748 genes in humans. U4atac/U6atac shares with U4/U6, despite sequence differences, a common secondary structure consisting of intra- and inter-molecular base-pairing. Some of the resulting domains such as Stem II and 5′ Stem-Loop bind essential splicing proteins. Most TALS patients carry homozygous or compound heterozygous mutations in the 5′ Stem-Loop, while all RFMN patients carry one of their two variants in Stem II, never found mutated in TALS (9). The physiopathological links between *RNU4ATAC* variants and TALS/RFMN/LWS symptoms remain largely

Significance

Introns must be removed from precursor messenger RNAs for proper eukaryotic gene expression. All major eukaryotic taxa have two types of introns, the major (>99%) and minor (<1%) introns, and two different ribonucleoprotein complexes to excise them, the major and minor spliceosomes. Biallelic mutations of *RNU4ATAC*, transcribed into the minor spliceosome component U4atac snRNA, were previously identified in patients presenting with three rare genetic syndromes combining variable intensity of microcephaly, growth restriction, bone anomalies, and immunodeficiency. Here, we shed light on a physiopathological mechanism underlying some *RNU4ATAC*-associated developmental anomalies by reporting biallelic *RNU4ATAC* mutations in five patients suspected of Joubert syndrome, a well-known ciliopathy. This finding is sustained by cellular and zebrafish models, thus linking minor splicing and primary cilium.

The authors declare no competing interest.

This article is a PNAS Direct Submission.

[1]D.K., A.P., S.M., and M.D. contributed equally to this work.

[2]To whom correspondence may be addressed. Email: marion.delous@inserm.fr.

This article contains supporting information online at https://www.pnas.org/lookup/suppl/doi:10.1073/pnas.2102569120/-/DCSupplemental.

Published February 21, 2023.

unknown. Although it has been shown that splicing defects affect most U12-type intron-containing genes (U12 genes) (3, 10, 11) to an extent that depends on the cell type (12), the resulting molecular perturbations causing the developmental anomalies have not been investigated yet, due to the lack of animal models and biological hypotheses.

In the present work, we report that pathogenic variants of *RNU4ATAC* may cause a disorder with overlapping traits of Joubert syndrome (JBTS), a well-known ciliopathy, characterized by developmental delay, dysregulation of the breathing pattern, hypoplasia of the cerebellar vermis, and a distinctive neuroradiologic "molar tooth sign" (MTS). This genetic finding made us consider an unsuspected link between minor splicing deficiency and cilium dysfunction, which we further confirmed both in patients' cells and in zebrafish model. Hence, *RNU4ATAC*-associated pathologies join the newly proposed group of "disorders with ciliary contribution".

Results

Identification of *RNU4ATAC* Mutations in Patients with JBTS-Like Traits. Two unrelated children suspected with having JBTS were referred to the genetic consultation. Targeted exome sequencing was performed, but no biallelic pathogenic variants or quantitative rearrangements were detected in known JBTS-related genes or other ciliary protein-encoding genes present on the Ciliome/CilDiag panels (*SI Appendix*, *Materials and Methods*). After modification of several bioinformatic parameters and the removal of a filter excluding noncoding genes, we identified in the two patients the same homozygous pathogenic variant, n.16G>A, in *RNU4ATAC* (GenBank: NR_023343) (Fig. 1*A* and *SI Appendix*, Table S1). Patient P1 (F1:II-2) exhibits an MTS, a severe developmental delay with severe axial hypotonia, microcephaly, skeletal dysplasia, facial dysmorphism, retinal coloboma, nystagmus, eczema, bilateral postaxial polydactyly, genital anomalies, growth hormone deficiency, small interventricular septal defect, and immunodeficiency (*SI Appendix*, Table S2). Patient P2 (F2:II-3), who died at 10 d of age, showed an MTS, microcephaly, skeletal dysplasia, an atrial septal defect, hand and foot abnormalities and ocular nystagmus (and strabismus) (*SI Appendix*, Table S2). Based on this discovery, we searched the presence of microcephaly and/or intrauterine growth retardation (IUGR) in a JBTS database of 183 patients without a molecular diagnosis after NGS analysis of a panel of 30 known JBTS genes. Six patients matching these criteria were identified and sequenced for *RNU4ATAC*. One of them presented

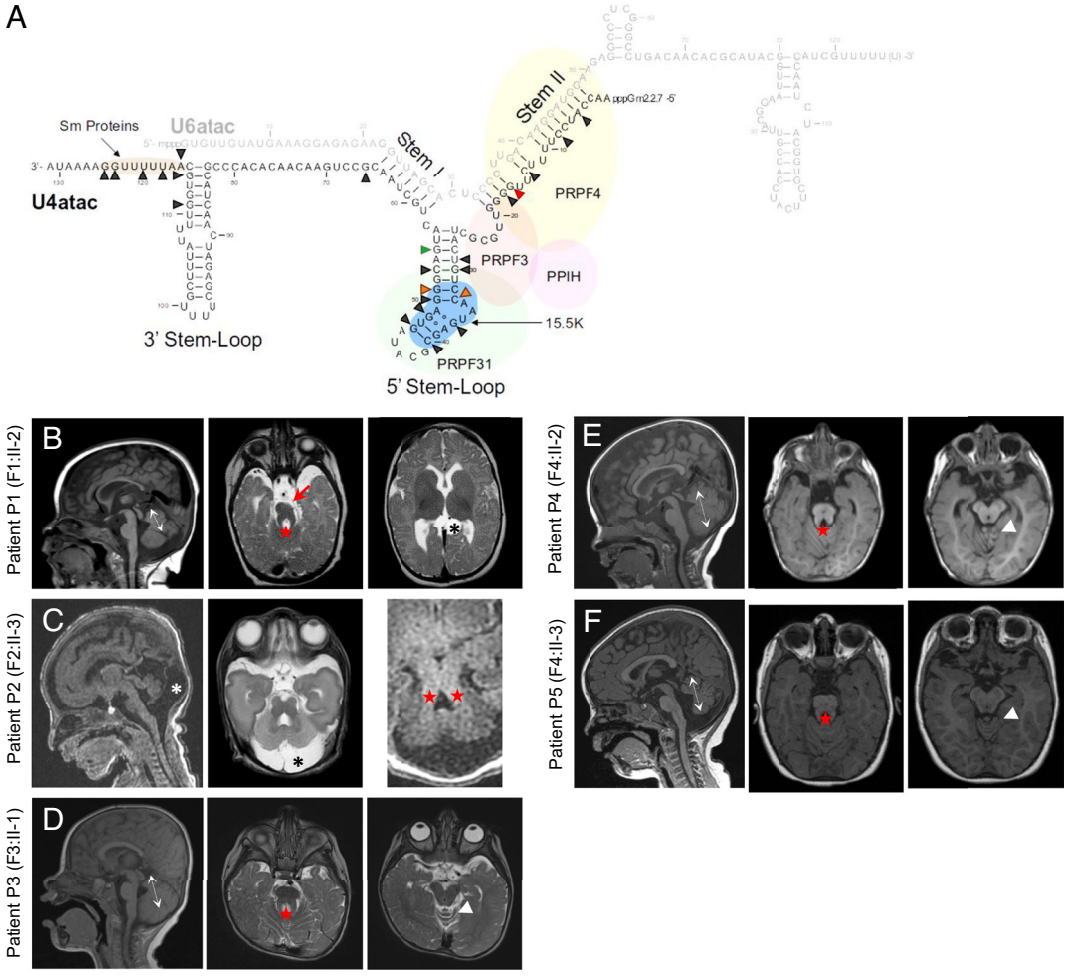

Fig. 1. *RNU4ATAC* is mutated in five cases of patients with JBTS-like traits. (*A*) Schema of the structure of the U4atac/U6atac bi-molecule with the main interacting proteins, showing with black arrowheads the nucleotides mutated in patients with *RNU4ATAC*-associated syndromes (9). The red arrowhead points to 16G [mutated in all five patients with JBTS-like disorder (n.16G>A)], the orange arrowheads to 33C and 51G [mutated in JBTS-like patients P3 (n.51G>A) and P4/P5 (n.33C>G)], the green arrowhead to 55G, the second most frequently mutated nucleotide after 51G in TALS patients. (*B*–*F*) Cerebral examination of all five *RNU4ATAC*-associated JBTS-like patients, performed at 7 mo of age for patient P1 (male, F1:II-2) (*B*), at 4 d of age in a premature baby born at 31.4 GW for patient P2 (female, F2:II-3) (*C*), at 1 y of age for patients P3 (female, F3:II-1) (*D*) and P4 (male, F4:II-2) (*E*), and at 2 y of age for patient P5 (female, F4:II-3) (*F*). Full descriptions of T1- or T2-weighted mid-sagittal (*Left*) and axial (*Middle* and *Right*) MRI are available in case reports, in *SI Appendix*. Main features: double arrows indicate vermian hypoplasia and/or dysplasia, asterisks arachnoid cyst, and red stars the « MTS ».

with the compound heterozygous variants n.[16G>A];[51G>A] (Fig. 1*A* and *SI Appendix*, Table S1). This patient, patient P3 (F3:II-1), is a 4-y-old girl who presents with an MTS, severe developmental delay with severe hypotonia, microcephaly, antenatal growth retardation, nystagmus, dysmorphism, and skeletal dysplasia (*SI Appendix*, Table S2). Finally, a 17-y-old boy and his 10-y-old sister (P4 and P5, F4:II-2 and F4:II-3) were referred for JBTS-like disorder and congenital left heart defect. Trio whole genome sequencing (WGS) was performed in P5 and her parents. No causative biallelic variants were found in JBTS-related genes (PanelApp: *Rare multisystem ciliopathy Super panel* v4.21) but compound heterozygous variants were detected in the *RNU4ATAC* gene: n.[16G>A];[33C>G] (Fig. 1*A* and *SI Appendix*, Table S1). Subsequently, Sanger sequencing confirmed the compound heterozygous status in her brother P4. The n.33>G variant, never reported in the literature nor in gnomAD v2.1.1, v3.1.2, ClinVar and HGMD® Professional 2022.1, is located in the most frequently mutated U4atac region, the 5′ Stem-Loop, in the K-turn motif that serves as a binding platform for the 15.5K protein. The genomic site and position show high conservation scores (PhyloP: 5,5; PhasCons: 1). Patients P4 and P5 present with an MTS, a psychomotor delay, ataxia, hypotonia, microcephaly, and nystagmus; additionally, P4 presents with IUGR and retinal dystrophy. Of note, congenital heart defect was also reported in the siblings: ventricular septal defect in both of them, as well as aortic coarctation in P4. Because the mother and a maternal uncle were also affected with aortic stenosis and aortic coarctation, respectively, a dominant congenital left heart cardiopathy is likely and the possibility of double diagnoses in this family is currently under investigation using WGS (*SI Appendix*, Table S2). All patients' brain MRI are shown in Fig. 1 *B*–*F*, with their detailed description in *SI Appendix* (case reports).

The n.16G>A variant, common to all five patients, was previously identified as pathogenic in typical RFMN patients (for whom no brain investigation has been reported), either at the compound heterozygous state in two pairs of siblings [in combination with n.51G>A (3) or n.46G>A (11)], or twice at the homozygous state (10, 11). Hence, taking into account this fact and the presence of both typical clinical features of the RFMN/TALS spectrum (at least microcephaly, with in some cases, growth retardation, skeletal dysplasia, and/or immunodeficiency) and of ciliopathies, i.e., cerebellar and brainstem anomalies suggestive of JBTS (all patients) and polydactyly in case of P1, we concluded that these patients exhibited overlapping phenotypic traits of both ciliopathy and *RNU4ATAC*-disease spectra, suggesting that *RNU4ATAC* loss of function secondarily results in ciliary defects.

MTS and Ciliopathy Traits Can Be Found in Other *RNU4ATAC*-Mutated Patients. This finding led us to conduct a thorough review of all *RNU4ATAC*-mutated published cases. We retrieved that an MTS had been noted in a TALS patient carrying the most frequent *RNU4ATAC* n.51G>A mutation at the homozygous state (13). Also, other ciliopathy-related traits had been observed in TALS/RFMN/LWS patients, notably retinitis pigmentosa, a cardinal feature of RFMN, and less frequently, polydactyly (TALS8 case) and cystic kidney (TALS10 case) (1). Atrial or ventricular septal defects, frequently observed in TALS/RFMN/LWS patients, are also a trait commonly found in ciliopathies (14), although not as specific as other phenotypes. Therefore, the presence of ciliopathy traits in other *RNU4ATAC* patients suggests that alteration of cilium structure/function is a possible mechanism downstream any mutations of *RNU4ATAC* and is not restricted to the presence of the n.16G>A pathogenic variant.

Cilium-Related Genes Are Overrepresented Among Human U12 Genes. To better apprehend the link between minor splicing and cilium function, we conducted a gene ontology (GO) enrichment analysis of U12 genes. Relatively few studies addressed the functions of U12 genes in recent years since their full identification has been facilitated both by the completion of the human genome sequence and the development of computational predictive tools. To the best of our knowledge, only three GO enrichment analyses have been performed, one based on functional gene sets and mouse phenotypes from the Mammalian Phenotype Ontology resource (3), one on the most differentially expressed U12 genes in adult human tissues (15), and the last on a subset of U12 genes associated with a disease (16). Here, we used a different approach and performed a GO term enrichment analysis of the U12 genes vs. the U2 genes, using the entire set of genes with GO annotations (n = 618 and 19,939 for U12 and U2 genes, respectively). An enrichment is observed if more than 3% (618/20,557) of U12 genes are present in a GO term. Hence, we found 243 enriched biological processes and 96 enriched cellular components with a *P* value ≤0.05 (Fig. 2*A* and Datasets S1). The most enriched biological process is the *membrane depolarization during action potential* (*P* value = 5.2e-15, with 42% of U12 genes), which partially overlaps the other GO terms *neuronal action potential* (*P* = 5.5e-13, 40%), *regulation of ion transmembrane transport* (*P* = 1.2e-12, 8%), *calcium ion transmembrane transport* (*P* = 4.3e-6, 9%), and *sodium ion transmembrane transport* (*P* = 5.2e-6, 10%). Interestingly, the *nonmotile cilium assembly* process (*P* = 6.8e-6, 18%) was the thirteenth most significant term (red in Fig. 2*A* and Dataset S1). Other significant terms explicitly related to cilia were identified, namely *intraciliary transport involved in cilium assembly* (*P* = 1.2e-3, 15%), *ciliary basal body-plasma membrane docking* (*P* = 1.6e-2, 7%), and *protein localization to ciliary transition zone* (*P* = 2.8e-2, 22%). Similarly, GO term enrichment analysis of cellular components revealed an unexpected amount of U12 gene-encoding proteins that localize at the basal body (*P* = 1.4e-5, 11%), the ciliary base (*P* = 4.3e-3, 14%), and the ciliary tip (*P* = 1.0e-2, 11%) (Dataset S1). Of note, the opposite comparison of U2 vs. U12 genes did not reveal any cilium-related terms (Dataset S1).

We then examined the broad class of cilium-related genes, bearing in mind that 2.0% of the genes contain a U12-type intron in the human genome (748 U12 vs. 37,173 U2 genes). Since we observed 7.6% (23 U12 genes vs. 279 U2 genes, Dataset S2) of U12 genes among the curated ciliary "Gold_Standard" genes (17), we concluded that there is an enrichment of U12 genes among them (hypergeometric test *P* value =1.0e-8). By broadening this list through the compilation of several databases (1,426 genes in total, see *Materials and Methods*), we identified 86 U12 genes (86/1426, 6%) (Fig. 2*B* and Dataset S2). Finally, among the 329 ciliopathy-related genes (18–20) (Dataset S2), 23 (~7%) are U12 genes (hypergeometric test *P* value = 5.2e-8). Strikingly, nearly a third of them are associated with JBTS (*ARMC9, CEP41, KATNIP, PDE6D, TCTN1, TCTN3, TMEM107, and TMEM231*) (Fig. 2*B* and Dataset S2), corresponding to 21.6% (8/37) of all known JBTS-associated genes.

Altogether, these enrichment analyses indicate that U12-type intron missplicing is likely to impair the expression of many genes crucial for cilium formation and/or function, thus suggesting a possible explanation for the ciliary contribution in *RNU4ATAC*-associated disorders.

n.16G>A *RNU4ATAC* Mutation Results in U12-type Intron Retentions . To validate the presence of intron retention (IR) in *RNU4ATAC*-associated JBTS-like patient cells, we conducted a transcriptomic study and qRT-PCR analyses. For this, we followed the approach we used in our in-depth analysis of transcriptomes of

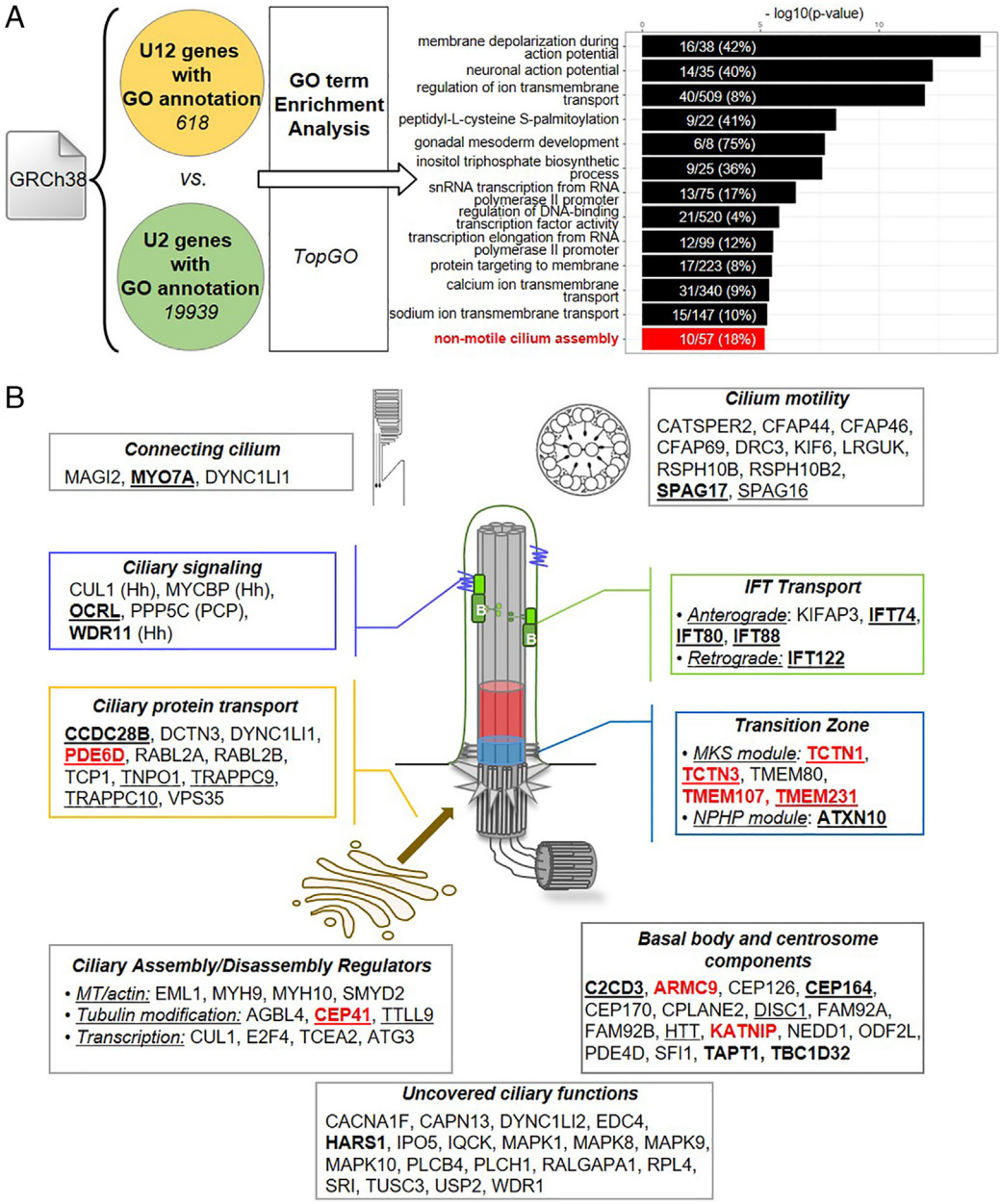

Fig. 2. The non-motile cilium assembly pathway is enriched among U12 genes. (*A*) GO term enrichment among U12-type intron-containing genes. Comparison of 618 U12 and 19,939 U2 genes with GO annotations, using the TopGO R package, allowed to identify 243 enriched biological processes with a *P* value ≤0.05, of which the 13 most significant are shown. Numbers in bars indicate the ratio of U12 genes belonging to each GO term (in brackets, the percentage). (*B*) Schema representing the localization and/or function of the 86 cilium-related U12 genes. Underlined are the "Gold_Standard" genes (17), in bold the genes associated with a ciliopathy, and in red those associated with JBTS. Hh, Hedgehog pathway; PCP, Planar Cell Polarity pathway.

three different cell types (fibroblasts, amniocytes, and lymphocytes) from seven TALS patients, which showed a specific and global alteration of minor splicing (U12-type IR mostly) while gene expression profiles were unchanged (12). Hence, the RNA-seq experiment carried out on fibroblasts derived from the skin biopsy of patient P1 revealed, like previously in TALS fibroblast samples (12), about the same amount of U12 expressed genes (~450), of which a small proportion (4%) showed differences of percent-spliced-in (dPSI) values of the U12-type intron greater than 10% (maximum dPSI of ~30%) compared to the control (Fig. 3*A* and Dataset S3). Most U12 introns (~96%) have a dPSI<10%, which suggests that fibroblasts are not the best-suited cell type to study minor spliceosome deficiency. The RNA-seq data indicate also that U12-type IR is not associated with drastic alterations of gene expression level (Dataset S3), as previously seen (12). We further analyzed U12-type IR in a few ciliary genes: *TMEM107, TMEM231,* and *TCTN1* that are JBTS-related genes with, respectively, high or low U12-type IR in TALS and P1 datasets; *RABL2A* that is a ciliary gene with a high dPSI in TALS dataset only; *IFT80* that is a ciliopathy gene with a null dPSI in both datasets. Sashimi plots, RT-PCR and qRT-PCR analyses of U12-type IR in these five genes showed for all of them a higher IR level in patients' cells than in controls, with a stronger effect seen in P1 compared to a TALS patient cell line (Fig. 3 *B–E* and *SI Appendix*, Fig. S1 *A* and *B*), although biological replicates (i.e., fibroblasts issued from other patients with n.16G>A homozygous mutation) would be needed to draw conclusions. It is noteworthy that qRT-PCR analyses evidence stronger IR than RNA-seq, particularly for *RABL2A* and *TMEM107*, which may be explained by the low coverage of their U12-type intron boundaries by NGS.

A dPSI	Number of expressed U12 genes		% of expressed U12 genes	
	TALS	P1	TALS	P1
≥ 10%	48	18	10	4
1 - 10%	275	140	57,4	30,8
< 1%	156	296	32,6	65,2
Total	479	454	100	100

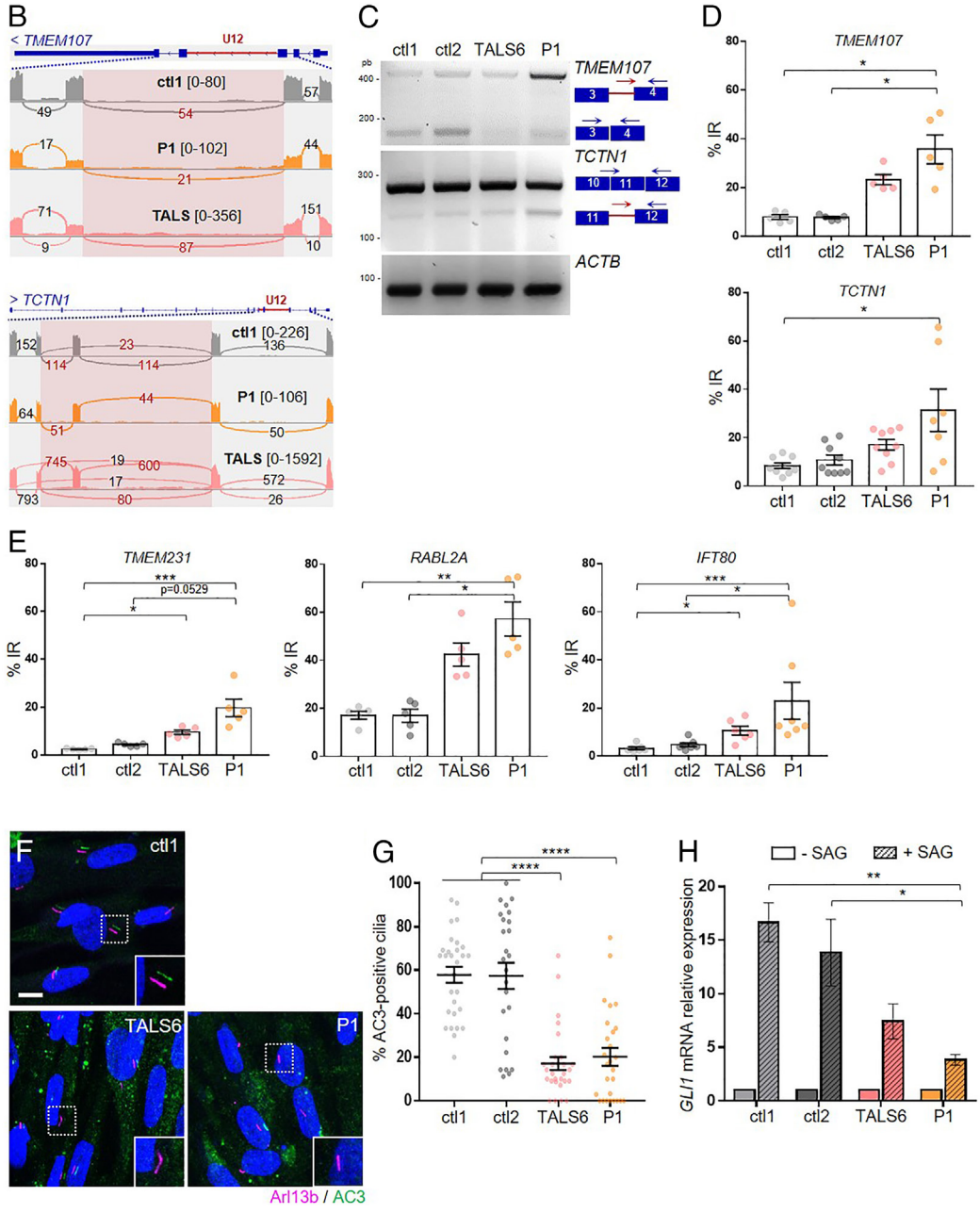

Fig. 3. JBTS-like and TALS *RNU4ATAC* mutations lead to U12-type IR in ciliary genes and result in ciliary function alteration in patient's fibroblasts. (*A*) Table summarising the results of the analysis of U12-type IR in the transcriptomic data of patient P1 vs. control (ctl1) fibroblasts, in the same format as those we previously published (12). Indicated are the number and percentage of U12 genes presenting differences of percent-spliced-in (PSI) values (dPSI) greater than 10%, between 10 and 1%, or below 1% between patient and control cells. (*B*) Sashimi plots of U12-type intron splicing of *TMEM107* and *TCTN1* genes, based on the present RNA-seq data of P1 and ctl1 fibroblasts, and on the previous pooled data of TALS fibroblasts (12). On lines, the number of reads split across splice junctions; in brackets, the range of coverage of each base of the depicted region. (*C*) RT-PCR using primers depicted in the schemas. *ACTB* is the actin beta housekeeping gene. (*D* and *E*) Graphs of qRT-PCR analyses showing the mean ± SEM of at least three independent experiments. Only significant comparisons are shown; **P* < 0.05, ***P* < 0.01, ****P* < 0.001 using Kruskal–Wallis test with Dunn's multiple comparisons. (*F*) Confocal images of an age- and sex-matched control, TALS6 and P1 patients' fibroblasts derived from skin biopsy. Shifted channels of adenylate cyclase (AC3, green) and Arl13b (cilium marker, magenta) staining are shown. (Scale bar, 10 µm.) (*G*) Quantification of the percentage of AC3-positive cilia seen in (*F*). Graphs show the mean ± SEM of at least 5 fields in five independent experiments (total number of analyzed cells >200). Only significant comparisons are shown; *****P* < 0.0001, using Kruskal–Wallis test with Dunn's multiple comparisons. (*H*) qRT-PCR analysis of the expression of the Hh target gene *GLI1* upon SAG treatment (+SAG). Graphs show the mean ± SEM of four to five independent experiments. Only significant comparisons are shown; ***P* < 0.01, **P* = 0.0499, using Kruskal–Wallis test with Dunn's multiple comparisons.

Altogether, these results confirmed that the n.16G>A mutation in P1 cells, similarly to other *RNU4ATAC* mutations associated with TALS, causes U12-type IR in patient fibroblasts, including in U12 ciliary genes.

Primary Cilium Function Is Altered in *RNU4ATAC*-Associated JBTS-Like and TALS Fibroblasts. To investigate whether U12-type IR had an impact on the centrosome structure and ciliogenesis, we studied patients' fibroblasts, a well-described and favored ciliated cell model, issued from JBTS-like patient P1 and from one TALS patient carrying the n.51G>A homozygous mutation [patient TALS6 described in Edery et al. (1)]. Analysis of the centrosome structure by ultrastructure expansion microscopy revealed no alteration of centriole composition; however, a slight increase of centriole length was observed in P1 fibroblasts (*SI Appendix*, Fig. S1 *C* and *D*). Regarding ciliogenesis, we analyzed the percentage of ciliated cells and cilium length, based on immunostainings of cilia with an antibody anti-Arl13b, which revealed slight ciliogenesis alterations in the TALS cell line but not in P1 patient cells (*SI Appendix*, Fig. S1 *E–G*). We then evaluated the cilium function and explored the ciliary localization of the protein adenylate cyclase III (AC3), which plays a crucial role in signal transduction of G-protein coupled receptors through the production of the second messenger cAMP. We observed a dramatic loss of AC3 into the cilium in TALS6 and P1 fibroblasts compared to the control cell lines (Fig. 3 *F* and *G*). We also explored Hedgehog (Hh) signaling, which is frequently altered in JBTS models. For this, we analyzed the expression of the target gene *GLI1* upon activation of the pathway with the smoothened agonist SAG. As compared to control cell lines, *GLI1* expression was twice less activated upon SAG treatment in both TALS6 and P1 fibroblasts (Fig. 3*H*). Hence, altogether, these results indicate that loss of U4atac function impairs primary cilium function (AC3-dependant cAMP signaling, Hh) rather than cilium formation. This could be explained by the fact that six U12 genes encode components of the transition zone, an essential filter barrier that controls the entry and exit of ciliary proteins in and out of the cilium.

Deficiency of u4atac in Zebrafish Leads to Ciliary Defects. To evaluate the importance of minor splicing during development, we turned to the zebrafish, a widely used animal model to study genetic diseases, including ciliopathies (21). Its genome includes 710 U12-type introns present in 655 genes in the latest genome assembly (GRCz11), as revealed by a computational scan that we performed using U12-type intron scoring matrices (22). These figures are in the same range as those found in humans, and most of the U12 zebrafish genes (544/655) are orthologs of human genes. Zebrafish has two orthologs for *RNU4ATAC*, and by combining the analysis of sequence and secondary structure conservation, expression throughout development, and phenotype of CRISPR/Cas9-mediated knockout lines (*SI Appendix*, Figs. S2 and S3), we concluded that *rnu4atac* on chromosome 11 was the sole functional ortholog of human *RNU4ATAC*.

Pathogenic variants in humans are hypomorphic and full deletion of rnu4atac_chr11 in zebrafish precluded the analysis of phenotypes beyond 22 hpf due to growth arrest and lethality (*SI Appendix*, Fig. S3*C*). We therefore opted for a morpholino-based approach and designed two morpholino oligonucleotides (MO) that targeted two distinct functional domains of u4atac, the 5′ Stem-Loop and Stem II (*SI Appendix*, Fig. S4*A*). Both MO led to a wide range of developmental anomalies whose severity was dose-dependent and concomitant with an increasing level of U12-type intron splicing deficiency (Fig. 4 *A–G* and *SI Appendix*, Fig. S4 *B–E*). Among the most penetrant phenotypes (>50% of MO-injected embryos), we observed body axis curvature, pronephric cysts, and otolith defects as well as cardiac dysfunction (Movies S1 and S2) and absence of touch response. To a lesser extent (<30%), u4atac morphants also exhibited microcephaly and brain hemorrhages (Fig. 4 *A–G* and *SI Appendix*, Figs. S4*D* and S5). All these phenotypes were rescued by the coinjection of human wild-type (WT) U4atac snRNA (Fig. 4*G* and *SI Appendix*, Figs. S4*D* and S5), in accordance with the highly similar bidimensional predictions of human U4atac/U6atac, zebrafish u4atac/u6atac, and human U4atac/zebrafish u6atac duplexes (*SI Appendix*, Fig. S2*D*). Strikingly, the three most penetrant phenotypes (i.e., body axis curvature, pronephric cysts, and otolith defects) are hallmarks of cilium dysfunction in zebrafish, thus strengthening the link between U4atac, minor splicing, and cilium function. For further evidence, we analyzed the cilium structure in the central canal (CC), pronephros, and otic vesicle (OV). Cilium dysfunction in the CC results in cerebrospinal fluid flow alteration and Reissner's fiber misaggregation, shown to be the origin of the ventral body curvature phenotype (23). In the pronephros, motile cilia, notably those of multiciliated cells, allow fluid flow in renal tubules; their impairment leads to fluid accumulation, tubule luminal expansion, and cyst formation in glomeruli (24). In the OV, motile cilia participate in otolith formation, favoring the binding of otolith precursor particles to the tip of kinocilia (25). We analyzed motile cilia in the CC by performing confocal live imaging of *Tg(bactin:arl13bGFP)* transgenic line. We observed a drastic decrease of cilium number in morphants (Fig. 4*H*), associated with defective cilium beating (Fig. 4 *H* and *H′*). In pronephros, we observed tubule dilations, mostly of the proximal straight tubule, that were accompanied by a lack of multiciliated tufts (Fig. 4*I*). Similarly, the number of cilia lining the OV was decreased (Fig. 4 *J* and *J′*). Finally, analysis of cilium formation at the nasal pit, at 48 hpf, revealed a significant alteration of the ciliary tuft in u4atac morphants compared to control embryos (Fig. 4*K*). All these ciliary defects were partially or totally rescued by the expression of human WT U4atac snRNA (Fig. 4 *G–K*).

Altogether, these data indicate that loss of function of u4atac is associated in vivo with ciliary defects, which are likely secondary to minor splicing alterations.

Ciliopathy-Related Phenotypes in Zebrafish Are Not Rescued by JBTS-Like and TALS U4atac Mutations. To have a better assessment of the impact of human U4atac variants on embryonic development processes linked to cilium function, we took advantage of the zebrafish model and conducted rescue experiments. We coinjected u4atac 5'SL MO with human U4atac carrying either the n.16G>A, n.51G>A, or n.55G>A mutation. These mutations have been identified at the homozygous state in 4, 31, and 8 patients or fetuses, respectively (9). They are associated with slightly different presentations (Dataset S4) and large differences in life expectancies: mean age at death is 10 mo for patients homozygous for n.51G>A (three surviving patients, ≤ 2 y old), while 3/4 and 4/8 of those with n.16G>A or n.55G>A were still alive at the time of publication at, respectively, 6, 6, and 38, or 2.5, 5.5, 9, and 18 y of age.

Stability of injected human U4atac snRNA was validated by Northern blot (*SI Appendix*, Fig. S4*F*), and the abovementioned phenotypes were recorded. We observed that 16A, 51A, and 55A snRNAs had little capacity to rescue the phenotype, with a gradation between their effect, 55A U4atac coinjected embryos having a slightly milder phenotype than those coinjected with 16A and 51A U4atac (Fig. 5 *A–C*). We also explored the impact of the mutations at the molecular level by analyzing in zebrafish the

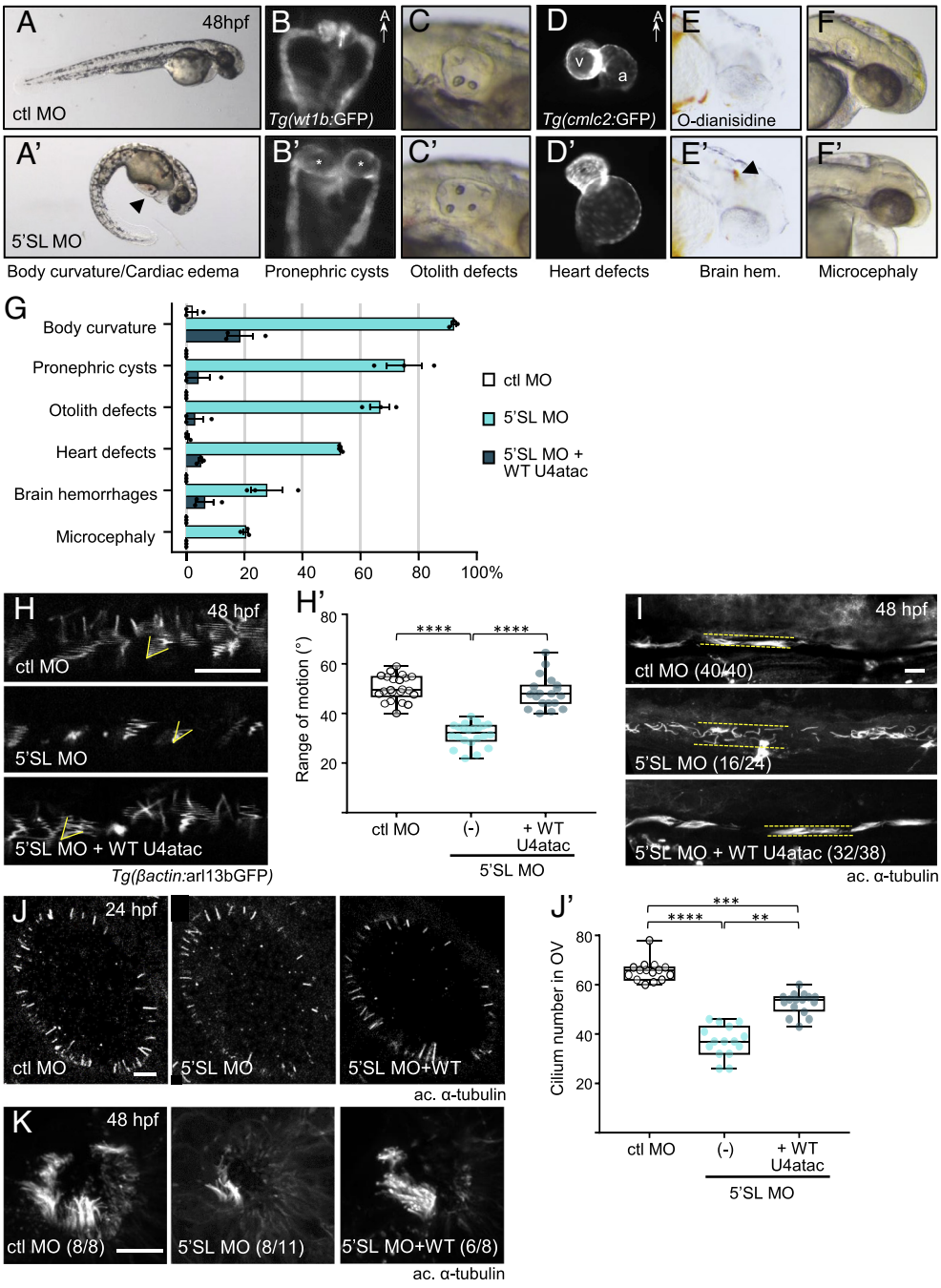

Fig. 4. Deficiency of u4atac leads to cilium alterations in zebrafish. (*A*–*F*) Global morphology of control (ctl) (*Upper*) and u4atac 5′SL (*Lower*) morpholino (MO)-injected embryos at 48 hpf. u4atac morphants are characterized by body curvature and cardiac edema (*A*′, arrowhead); cysts (*B*′, asterisks) in glomeruli; anomalies of otoliths in OV (*C*′); alterations of cardiac morphology (*D*′); blood hemorrhages in brain (*E*′, arrowhead); and microcephaly (*F*′). Dorsal views in *B* and *B*′ and ventral views in *D* and *D*′, with anterior to the top. (*G*) Percentage of embryos displaying each of the phenotypes shown in *A*′–*F*′, following injection of control MO, u4atac 5′SL MO alone or with human WT U4atac snRNA. Graph shows the mean ± SEM of three independent experiments (total number of embryos >300). $P < 0.01$, *t*-tests comparing 5′SL MO to ctl MO, and 5′SL MO + WT to 5′SL MO. (*H*) Live confocal imaging of motile cilia in CC of MO-injected *Tg(bactin:arl13bGFP)* transgenic embryos, at 48 hpf. Slow acquisition speed of motile cilia produces imaging artifacts, delineating the range of motion of each cilium (yellow angles). (*H*′) Quantification of the angle of motile cilium range of motion in control MO (n = 22), u4atac 5′SL MO alone (n = 22), or with human WT U4atac snRNA (n = 20) injected embryos, as described in (*H*). (*I*–*K*) Immunostaining of cilia (acetylated α-tubulin) in the proximal straight tubule (*I*), the OV (*J*), and at the nasal pit (*K*) of control MO, u4atac 5′SL MO alone, or with human WT U4atac snRNA injected embryos, at 24 (*J*) or 48 (*I* and *K*) hpf. In brackets, the number of embryos exhibiting the phenotype shown in the image over the total number of analyzed embryos. Dotted lines in *I* delineate the tubule lumen. (*J*′) Quantification of the cilium number in OV of control MO (n = 15), u4atac 5′SL MO alone (n = 15), or with human WT U4atac snRNA (n = 16) injected embryos, as described in (*J*). For quantification (*H*′ and *J*′), box-and-whisker plots show in the box the median and the 25th to 75th percentiles and in whiskers the minimum to the maximum values, which were obtained in two independent experiments. For *H*′, values are the mean range of motion of all cilia measured in one single embryo. Only significant comparisons are shown; ****$P < 0.0001$, ***$P < 0.005$, **$P < 0.01$ by Kruskal–Wallis test with Dunn's multiple comparisons test. Images show the maximum intensity projection (*H*, *I*, *K*) or a single optical slice selected in the middle of z-stack (*J*). (Scale bars, 10 μm.) a, atrium; v, ventricle; hem, hemorrhages.

U12-type IR of six cilium-related genes (*rabl2, tmem107l, tmem231, ift80, tctn1*, and *pde6d*), among which the five genes tested in TALS6 and P1 patients' cells. For all of them, the U12-type intron was strongly retained in 5′SL MO-injected embryos, and mis-splicing could be rescued to the level of control by the coinjection of WT U4atac. Consistent with the observed

phenotype, n.55G>A had a lower impact on minor splicing than n.51G>A and n.16G>A (Fig. 5*D*).

In conclusion, JBTS-like and TALS *RNU4ATAC* pathogenic variants all lead to ciliary defects in zebrafish, due to a deficiency of minor splicing. Of note, we observed that variants may have variable impacts, sustaining a phenotype/genotype correlation that will need to be further explored.

Discussion

We report here the identification, in five cases suspected of having JBTS, of biallelic pathogenic variants of *RNU4ATAC*, a gene previously involved in three rare syndromes (TALS, RFMN, and LWS) characterized by microcephaly, short stature, and other specific features. In line with this finding, we found that cilium-related genes are overrepresented among human U12 genes, that several ciliary genes are impacted by defective minor splicing and that primary cilium function is altered in TALS and JBTS-like fibroblasts. Furthermore, the zebrafish *u4atac* models present with ciliopathy-related phenotypes and ciliary defects that could be rescued by WT but not by U4atac carrying TALS and JBTS-like variants.

Quite remarkably, the five patients we describe here have a complex syndromic disorder combining some traits seen in both JBTS patients (MTS, hypotonia, nystagmus/strabismus, and polydactyly/clinosyndactyly) and TALS/RFMN/LWS patients (microcephaly, skeletal dysplasia, growth retardation, immunodeficiency, and eczema). These five patients all carry n.16G>A. Siblings P4 and P5 carry as well in trans a new *RNU4ATAC* variant, n.33C>G, while the genotype of P3, n.[16G>A];[51G>A], has already been reported in two RFMN siblings (3), who were initially thought to have nonasphyxiating Jeune syndrome (a ciliopathy) on the basis of their bone dysplasia, dysmorphic features, and hepatic involvement (26) (*SI Appendix*, Table S2). Two unrelated patients, P1 and P2, are homozygous for n.16G>A; it should be noted that this variant is the only one in Stem II previously found at the homozygous state, and this in two typical RFMN patients [a 6-y-old girl (10) and a 38-y-old male (11)]. It is noteworthy that one of them presented with "eye motility problems" (*SI Appendix*, Table S2) (11), a feature previously unseen in *RNU4ATAC*-associated pathologies but that can correlate with ophthalmologic anomalies seen in JBTS. As for the MTS, most RFMN patients present with a mild microcephaly and borderline-to-mild intellectual impairment, so that brain MRI is rarely performed. Based on our findings, we suggest that the four previously published RFMN patients with the same genotypes than three of our patients should have a thorough investigation of their brain morphology to explore the possible presence of an MTS. Conversely, patients P3 to P5 should have a thorough investigation of their immunological profile to investigate a potential immune dysfunction.

As ciliopathy-related traits have been observed in some TALS/RFMN/LWS patients [including an MTS in one of them, (13)], the overlap with ciliopathies is clearly not restricted to *RNU4ATAC*-associated JBTS-like cases, even if it might be greater for n.16G>A carriers. In agreement with this, a recent disease-scoring system based on the occurrence of ciliopathy-like phenotypes produced high scores for RFMN and TALS (respectively, 267th and 428th highest scores among 6,058 analyzed disorders), making them likely candidates for disorders with ciliary contribution (18).

Additional evidence is provided by the zebrafish *u4atac* model. As seen in patients, MO-mediated deficiency of u4atac led to phenotypes that recapitulate features both associated with TALS/RFMN/LWS [microcephaly, brain hemorrhages (13, 27), and cardiac defects] and with ciliopathies (body axis curvature, pronephric cysts, and otolith defects). Brain hemorrhages could even fall in this last category as they have been shown to result from ciliary defects of endothelial cells in zebrafish (28, 29). Our results demonstrate that the ciliopathy-related phenotypes are indeed due to ciliary defects in the CC, pronephros, OV, and olfactive bulb. These phenotypes could be mostly rescued by coinjection of the human WT U4atac snRNA but not, or to a lesser extent, by snRNA molecules carrying JBTS-like or TALS-associated mutations. These results thus strongly support the fact that several types of pathogenic variants of *RNU4ATAC* can result in ciliopathy-related phenotypes.

By identifying biallelic *RNU4ATAC* mutations in five patients with ciliopathy traits, we shed light on a new "second-order" mechanism leading to ciliary defects, i.e., splicing of minor introns. Second-order ciliopathies are caused by mutations in genes that have an indirect role in cilium formation or function (19). Alterations of (major) splicing have already been associated with ciliopathies, with notably the identification of mutations in several genes encoding protein components of the spliceosomes in patients with retinitis pigmentosa, such as PRPF31 to cite only one (30). Whether it be splicing (30, 31) or other steps of RNA metabolism operated by the RNA helicase DDX59 or the RNA-binding protein BICC1, involved in Oro-Facial-Digital syndrome and cystic renal dysplasia, respectively (32, 33), it remains to explain why ciliary genes are specifically affected and how they drive the phenotype. In the case of minor splicing, the high proportion of U12 genes encoding ciliary components (at least 86, i.e., 12% of the total number of U12 genes) is likely to be an important factor, combined to the fact that the cilium is a complex sensory machine involved in transducing a wide range of extracellular stimuli into cellular responses essential for organogenesis. Further investigations are needed to address these questions, taking into account that defective minor splicing results in much more complex outcomes than the simply decreased expression of genes with U12-type IR (due to reduced abundance of canonical protein-coding isoforms). A recent review pointed out the crosstalk mechanisms between major and minor spliceosomes, that may vary depending on cell type and throughout development (34). Global transcriptomic analyses of splicing events are thus definitely needed to understand the impact of *RNU4ATAC* mutations, and these studies will be carried out in the zebrafish model, as well as in human development models derived from induced pluripotent stem cells.

To conclude, our work is of significant impact for both JBTS-like and TALS/RFMN/LWS patients, notably regarding the genetic diagnosis and counseling. Due to its noncoding status, *RNU4ATAC* is still underconsidered among the clinically relevant genes. Not only should it be evaluated in the JBTS-like cases lacking a molecular diagnosis, but given the pleiotropy of the clinical signs associated with this gene, one should remain open when assessing its potential pathogenic variants in patients with rare diseases. Also, our work widens the fields of research on the physiopathological mechanisms underlying the *RNU4ATAC*-associated diseases.

Materials and Methods

Molecular Diagnostic Analyses. For patients P1 and P2, a targeted sequencing of genes involved in ciliary diseases or cilium function was performed using custom SureSelect capture kits [CilDiag (170 genes) for P1, Ciliome V3c (1,339 genes) (35, 36) for P2] (Agilent Technologies, Santa Clara, CA, USA), and HiSeq or NextSeq sequencers (Illumina, San Diego, CA, USA), respectively. Since the analysis of coding gene sequences did not reveal any biallelic variants in one gene (*SI Appendix*), variants in noncoding genes were next analyzed, allowing the identification of biallelic *RNU4ATAC* mutations. All variants identified by NGS were confirmed by Sanger sequencing. For patient P3, the single exon of *RNU4ATAC* was PCR-amplified and Sanger sequenced using one primer pair

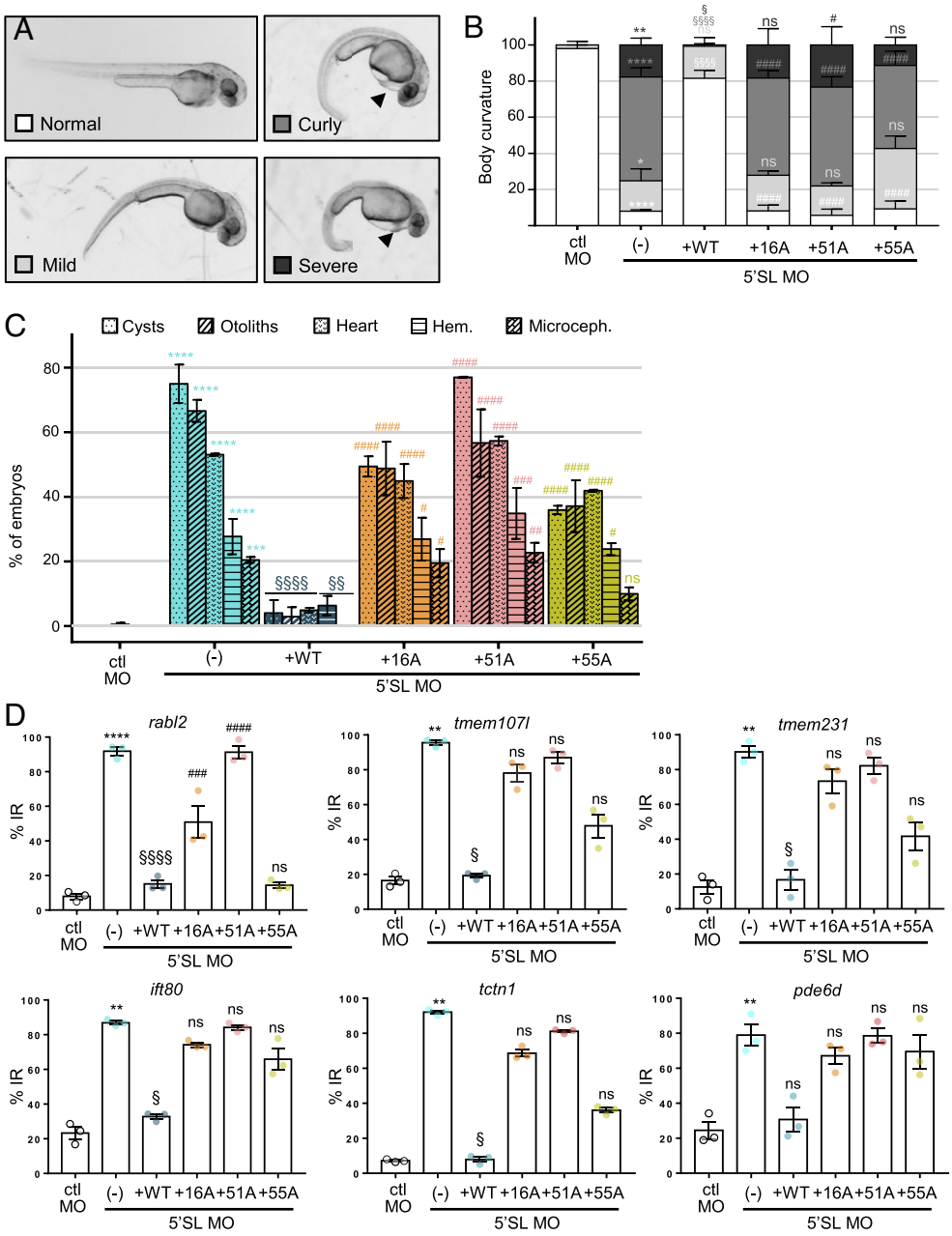

Fig. 5. Coinjected JBTS-like and TALS U4atac mutants lead to ciliopathy-related phenotypes in zebrafish. (*A*) Global morphology of embryos coinjected with 5'SL MO and JBTS-like (16A) or TALS (51A, 55A)-related U4atac variants. A varying severity of body curvature could be observed (mild, curly, severe), as well as the presence of cardiac edema (black arrowhead). (*B* and *C*) Percentage of embryos exhibiting the various severities of body curvature (*B*) shown in (*A*), and each of the phenotypes (*C*) shown in Fig. 4 *A*–*F*, following coinjection of 5'SL MO with human WT or mutated U4atac snRNA. Graphs show the mean ± SEM of three batches of 60 embryos issued from independent experiments (total number of embryos: 180). Statistical analysis with ctl MO (*), 5'SL MO (§), or 5'SL MO+WT hU4atac (#). ****$P < 0.0001$, ***$P < 0.001$, **$P < 0.01$, *$P < 0.05$, ns nonsignificant, by two-way ANOVA test with Sidak's (*, §) or Dunnett's (#) multiple comparisons test. (*D*) qRT-PCR analysis of U12-type IR in six cilium-related genes in embryos coinjected with 5'SL MO and human WT or mutated U4atac snRNA. Graphs show the mean ± SEM of three independent experiments. Statistical analysis with ctl MO (*), 5'SL MO (§), or 5'SL MO+WT hU4atac (#). ****$P < 0.0001$, ***$P < 0.001$, **$P < 0.01$, *$P < 0.05$, ns nonsignificant, by Kruskal–Wallis test with Dunn's multiple comparisons test.

(*SI Appendix*, Table S3). For P5, a WGS was performed at the SeqOIA Lab (Plan France Médecine Génomique 2025, Paris, France) (see details in *SI Appendix*). The segregation of the variants identified in patient P5 was verified in her brother, patient P4, using Sanger sequencing as for patient P3.

Bioinformatic Analyses. U12 genes were identified by running the U12db (22) annotation pipeline on the GRCh38 version of the human genome, with the gencode38 version of the annotations, or the GRCz11 version of the zebrafish genome. GO term analysis was performed with the TopGO (v2.38.1) R tool (37), with the default "weight01" algorithm, the Fisher-test and the org.Hs.eg.db (v3.10.0) R database of the genome-wide annotation for humans. Genes without any GO annotation were discarded.

To constitute a list of cilium-related genes, we combined three existing databases and defined a gene as cilium-related if 1) it was part of the Gene_Ontology (GO = Cilium) of the Gold_Standard (SysCilia, a curated list of known ciliary components) (17) or of the Predicted candidates based on a bayesian integration in CiliaCarta (38) (last updated version of March, 18th 2018); 2) it was in the CilDB table v3.0 and had the maximum human ciliary evidence stringency level and at least 3 ciliary evidence (39, 40) (last update June 2014); and 3) it was a ciliopathy-related gene (18–20).

Cell Culture and Immunofluorescence. Primary human fibroblasts were cultivated in HAM-F10 media (Eurobio, CM1H1000-01) supplemented with 12% FBS and 1% penicillin-streptomycin. To induce ciliogenesis, cells were starved (HAM-F10 + 0.5% FBS) for 2 d. To activate the Hh pathway, Smoothened Agonist (SAG, 566660,

Merck Millipore) was added at 800 nM during the last 24 h of serum starvation. Cells were fixed in 4% PFA or with cold methanol during 20 min at room temperature and saturated with blocking buffer (PBS 1X, 10% goat serum, 1% BSA, 0.1% Triton) for an hour. The following primary antibodies were used: Arl13b (1:500, 17711-1 AP, Proteintech), γ-tubulin (1:250, ab11316, Abcam), acetylated α-tubulin (1:1,000, T6793, Sigma), and AC3 (1:500, PA5-35382, Invitrogen), diluted in blocking buffer and incubated overnight at 4 °C. After several washes with PBS, secondary antibodies (1:1,000, A32731, A32728, Invitrogen) were incubated for 1.5 h, followed by DAPI for 10 min, prior to coverslip mounting using FluorPreserveTM Reagent (EMD Millipore, 3457870). Z-stack images were taken using a Zeiss LSM880 confocal microscope, and measurement of the cilium length was performed manually on images of maximum intensity projection of z-stacks, using ImageJ software.

Zebrafish Husbandry and Microinjection of Embryos. Zebrafish (*Danio rerio*) adults and embryos were maintained at 28.5 °C under standard protocols (41). The following strains were used: the mixed wild-type ABxTU, *Tg(wt1b:EGFP)li1* (42), *Tg(cmlc2:GFP),* and *Tg(bactin:arl13bGFP)hsc5Tg* (43) to label proximal pronephros, heart, and cilia, respectively. MO, designed to target the 5′ Stem-Loop (5′SL) (5′-GATGTTCTCAGTTAACCTTCATTGA-3′) or the Stem II (SII) (5′-AAACCACCCCCAGACAAGGAA-GGTT-3′) regions of u4atac_chr11, were provided by GeneTools, LCC and injected into the yolk at the one-cell stage (quantity ranging from 0.016 to 0.066 pmol (i.e., 135 to 556 pg) per embryo for 5′SL MO and 0.002 to 0.006 pmol (i.e., 17 to 51 pg) per embryo for SII MO). A five-mismatch MO (5′-GATcTTgTCAcTTAACCTTgATTgA-3′) was used as a negative control. For rescue experiments, snRNA molecules were synthesized using the MAXIscript T7 Transcription Kit (ThermoFisher Scientific); DNA templates of human U4atac snRNA sequence were PCR-amplified from previously described plasmids (9) (*SI Appendix*, Table S3). snRNA molecules were purified with Clean and Concentrator kit (Zymo Research), and 65 pg were coinjected with u4atac MO per embryo.

RNA extraction, RT-PCR, and qRT-PCR. Total RNA was extracted from cultured fibroblasts or a pool of 20 zebrafish embryos and treated with DNase I using NucleoSpin RNA plus kit (Macherey-Nagel). Then, 1.5 μg of total RNA was retro-transcribed into cDNA [GoScript Reverse Transcriptase (Promega)] using random hexamers or oligodT. RT-PCR was performed using the GoTaq Green Master Mix (Promega) and RT-qPCR using the Rotor-gene Q (Qiagen), following both manufacturers' instructions. For RT-qPCR, the reactions were performed in triplicate, with the appropriate primers and *ACTB* for fibroblasts or *gapdh* for zebrafish as reference genes (*SI Appendix*, Table S3). Relative levels of expression of *rnu4atac* genes were calculated using the $2^{-\Delta\Delta Ct}$ method; the percentage of IR is the ratio of unspliced transcript level to that of the total of unspliced and spliced forms, after normalization to the level of *ACTB*/*gapdh* gene expression.

Zebrafish Whole Mount Immunostaining and Imaging. Dechorionated embryos were washed in PBS, fixed in 4% PFA overnight prior to yolk removal. After 3-h incubation in blocking solution (PBS+0.1% Tween20 (PBST), 3% BSA), embryos were washed thrice in PBST and incubated overnight at 4 °C with anti-acetylated α-tubulin antibody in PBST (1:500, T6793, Sigma). Embryos were then extensively washed and incubated with Phalloidin–tetramethylrohdamine B isothiocyanate (1:100, P1951, Sigma) for 20 min at room temperature, before being washed and incubated again overnight at 4 °C with anti-mouse secondary antibody in PBST (1:2,000, A32728, Invitrogen). Finally, embryos were mounted on glass slides using FluoPreserveTM Reagent (Merck) prior to confocal imaging using Zeiss LSM880 microscope. Live embryos were mounted in 0.4 % low-melting agarose mixed with Tricain in glass-bottom Petri dishes (Ibidi). Beating cilia were imaged by optimizing the signal-to-noise ratio and the scan speed, as previously described (43). Z-stacks were performed to acquire the whole organs and quantification of cilium number, and range of motion was done manually and blinded on images of maximum intensity projection of z-stacks, using ImageJ software.

Statistics. All the data are reported as the mean of at least three independent experiments with SEM. All hypothesis tests were two-sided, and statistically significant differences ($P < 0.05$) were calculated by one-way ANOVA or *t* tests as indicated in figure legends. When the sample size was too small or when normality was not reached (following the Shapiro–Wilk test), a nonparametric test was used. Statistical analyses were performed using GraphPad Prism software.

Study Approval. Written informed consent was obtained from parents for the genetic study and for the publication of clinical information. The study on patient' cells was approved by the French national ethical committee Comité de Protection des Personnes (number 2021-A01551-40). Animal studies (zebrafish) were conducted in accordance with the European regulations on animal use.

Data, Materials, and Software Availability. Raw RNAseq data: The consent form signed by the parents of the child whose RNA was sequenced does not include agreement to dataset deposition on public databases. Therefore, as stated in the manuscript, the raw sequencing data can be obtained upon request.

ACKNOWLEDGMENTS. We thank the families for their contribution to this project. We thank the Centre de Biotechnologie Cellulaire Biotec biobank for biosample management (Emilie Chopin, Isabelle Rouvet), the Plateau de Recherche Expérimentale en Criblage In vivo aquatic core facility (Laure Bernard, Robert Renard), the Tefor facility, and the Gendev team members for stimulating discussions. This work was supported by CNRS, Inserm, Université de Montpellier, Université Paris 7 and Université Lyon 1 through recurrent funding; the Fondation Maladies Rares ("Small Animal Models and Rare Diseases" program, no. 20161207); the Agence Nationale de la Recherche (no. ANR-18CE12-0007-01); and the Fondation pour la recherche sur le Cerveau « Espoir en tête » (confocal microscope). E.B. was supported by an European Molecular Biology Organization long-term fellowship (ALTF-284-2019) and the Novartis Foundation for medical-biological Research (18B112).

Author affiliations: [a]Université Claude Bernard Lyon 1, INSERM, CNRS, Centre de Recherche en Neurosciences de Lyon CRNL U1028 UMR5292,Genetics of Neurodevelopment Team, 69500 Bron, France; [b]Department of Genetics, Clinical Genetics Unit, Centre de Référence Maladies Rares des Anomalies du Développement, Hospices Civils de Lyon, Université Claude Bernard Lyon 1, 69500 Bron, France; [c]Institut national de recherche en sciences et technologies du numérique Erable, Laboratoire de Biométrie et Biologie Evolutive, UMR5558 CNRS, Université Claude Bernard Lyon 1, 69622 Villeurbanne, France; [d]Department of Histology Embryology and Cytogenetics, Assistance Publique - Hôpitaux de Paris, Necker-Enfants Malades Hospital, University of Paris, 75015 Paris, France; [e]Department of Cell Biology, Sciences III, University of Geneva, 1211-Geneva, Switzerland; [f]Laboratory of hereditary kidney diseases, Imagine Institute, U1163 INSERM, University of Paris, 75015 Paris, France; [g]Département de Génétique, Centre de Référence des Malformations et Maladies Congénitales du Cervelet, Assistance Publique - Hôpitaux de Paris, Sorbonne University, Trousseau Hospital, 75012 Paris, France; [h]Department of Genetics, Clinical Genetics Unit, Centre de Compétence Anomalies du Développement et Syndromes Polymalformatifs, Centre Hospitalier Universitaire Morvan, 29200 Brest, France; [i]Laboratoire SeqOIA–PFMG2025, 75014 Paris, France; [j]Hematology-Immunology Unit, Assistance Publique - Hôpitaux de Paris, Necker-Enfants Malades Hospital, 75015 Paris, France; [k]Pediatric service, Centre Hospitalier Morlaix, 29600 Morlaix, France; [l]Clinical Genetics Unit, Maternité Port-Royal, Assistance Publique - Hôpitaux de Paris, Cochin Broca Hôtel-Dieu Hospitals 75014 Paris, France; [m]Neonatal and Pediatric Units, Louis-Mourier Hospital, 92700 Colombes, France; [n]Pediatric and Fetal Imaging, Hospices Civils de Lyon, Université Claude Bernard Lyon 1, 69500 Bron, France; [o]Clinical Genetics Department, Centre de Référence Maladies Rares–Maladies Osseuses Constitutionnelles, Assistance Publique - Hôpitaux de Paris, Necker-Enfants Malades Hospital, 75015 Paris, France; [p]Developmental Brain Disorders Laboratory, Imagine Institute, U1163 INSERM, University of Paris, 75015 Paris, France; [q]Service de Génétique Clinique, Centre Hospitalier Universitaire Rennes, Centre de référence Anomalies du développement et syndromes malformatifs, Univ Rennes, CNRS, INSERM, Institut de Génétique et Développement de Rennes UMR 6290/ Equipe de Recherche Labellisée 1305, 35000 Rennes, France; [r]NeuroDiderot, UMR1141, University of Paris, 75019 Paris, France; [s]Departement of Genetics, Assistance Publique - Hôpitaux de Paris, Robert Debré Hospital, 75019 Paris, France; [t]Pediatric Service, Centre Hospitalier Régional Universitaire Brest, 29200 Brest, France; and [u]Institute of Molecular Genetics of Montpellier, UMR5535 CNRS, University of Montpellier, 34000 Montpellier, France

Author contributions: V.H., L.B., S.M., and M.D. designed research; D.K., A.C., S.K., A.B., E.B., J.G., A.F., M.A.D., R.B., and M.D. performed research; D.K., A.C., S.K., A.B., E.B., J.G., A.F., M.A.D., C.B.-P., L.Q., S.A.-E, P.B., T.R., L.G., V.H., R.B., A.-L.L., , L.B., T.A.-B., and M.D. analyzed data; A.P., S.A.-B., M.C., G.C., S.G., A.G., L.G., C.M., S.O., L.R., E.S., and P.E. did clinical examination; and A.P., A.C., S.O., L.B., S.M., and M.D. wrote the paper.

The manuscript was deposited in medRxiv (https://doi.org/10.1101/2021.12.12.21266616).

1. P. Edery *et al.*, Association of TALS developmental disorder with defect in minor splicing component U4atac snRNA. *Science* **332**, 240–243 (2011).
2. H. He *et al.*, Mutations in U4atac snRNA, a component of the minor spliceosome, in the developmental disorder MOPD I. *Science* **332**, 238–240 (2011).
3. D. Merico *et al.*, Compound heterozygous mutations in the noncoding *RNU4ATAC* cause Roifman syndrome by disrupting minor intron splicing. *Nat. Commun.* **6**, 8718 (2015).
4. L. S. Farach *et al.*, The expanding phenotype of *RNU4ATAC* pathogenic variants to Lowry wood syndrome. *Am. J. Med. Genet. A* **176**, 465–469 (2018).

5. H. Hagiwara *et al.*, Immunodeficiency in a patient with microcephalic osteodysplastic primordial dwarfism type I as compared to Roifman syndrome. *Brain Dev.* **43**, 337–342 (2020).
6. A. Putoux *et al.*, Refining the phenotypical and mutational spectrum of Taybi-Linder syndrome. *Clin. Genet.* **90**, 550–555 (2016).
7. J. J. Turunen, E. H. Niemela, B. Verma, M. J. Frilander, The significant other: Splicing by the minor spliceosome. *Wiley Interdiscip. Rev. RNA* **4**, 61–76 (2013).
8. G. E. Larue, M. Elias, S. W. Roy, Expansion and transformation of the minor spliceosomal system in the slime mold Physarum polycephalum. *Curr. Biol.* **31**, 3125–3131.e4 (2021).
9. C. Benoit-Pilven *et al.*, Clinical interpretation of variants identified in *RNU4ATAC*, a non-coding spliceosomal gene. *PLoS One* **15**, e0235655 (2020).
10. Y. Dinur Schejter *et al.*, A homozygous mutation in the stem II domain of *RNU4ATAC* causes typical Roifman syndrome. *NPJ Genom. Med.* **2**, 23 (2017).
11. J. Heremans *et al.*, Abnormal differentiation of B cells and megakaryocytes in patients with Roifman syndrome. *J. Allergy Clin. Immunol.* **142**, 630–646 (2018).
12. A. Cologne *et al.*, New insights into minor splicing-a transcriptomic analysis of cells derived from TALS patients. *RNA* **25**, 1130–1149 (2019).
13. G. M. Abdel-Salam *et al.*, Further delineation of the clinical spectrum in *RNU4ATAC* related microcephalic osteodysplastic primordial dwarfism type I. *Am. J. Med. Genet. A* **161A**, 1875–1881 (2013).
14. O. Burnicka-Turek *et al.*, Cilia gene mutations cause atrioventricular septal defects by multiple mechanisms. *Hum. Mol. Genet.* **25**, 3011–3028 (2016).
15. A. M. Olthof, K. C. Hyatt, R. N. Kanadia, Minor intron splicing revisited: Identification of new minor intron-containing genes and tissue-dependent retention and alternative splicing of minor introns. *BMC Genom.* **20**, 686 (2019).
16. A. M. Olthof, J. S. Rasmussen, P. M. Campeau, R. N. Kanadia, Disrupted minor intron splicing is prevalent in Mendelian disorders. *Mol. Genet. Genomic Med.* **8**, e1374 (2020).
17. T. J. van Dam *et al.*, The SYSCILIA gold standard (SCGSv1) of known ciliary components and its applications within a systems biology consortium. *Cilia* **2**, 7 (2013).
18. M. Lovera, J. Luders, The ciliary impact of nonciliary gene mutations. *Trends Cell Biol.* **31**, 876–887 (2021).
19. J. F. Reiter, M. R. Leroux, Genes and molecular pathways underpinning ciliopathies. *Nat. Rev. Mol. Cell Biol.* **18**, 533–547 (2017).
20. G. Wheway, H. M. Mitchison; Genomics England Research Consortium, Opportunities and challenges for molecular understanding of ciliopathies-The 100,000 genomes project. *Front. Genet.* **10**, 127 (2019).
21. Z. Song, X. Zhang, S. Jia, P. C. Yelick, C. Zhao, Zebrafish as a model for human ciliopathies. *J. Genet. Genom.* **43**, 107–120 (2016).
22. T. S. Alioto, U12DB: A database of orthologous U12-type spliceosomal introns. *Nucleic Acids Res.* **35**, D110–D115 (2007).
23. Y. Cantaut-Belarif, J. R. Sternberg, O. Thouvenin, C. Wyart, P. L. Bardet, The Reissner fiber in the cerebrospinal fluid controls morphogenesis of the body axis. *Curr. Biol.* **28**, 2479–2486.e4 (2018).
24. A. G. Kramer-Zucker *et al.*, Cilia-driven fluid flow in the zebrafish pronephros, brain and Kupffer's vesicle is required for normal organogenesis. *Development* **132**, 1907–1921 (2005).
25. D. Wu, J. B. Freund, S. E. Fraser, J. Vermot, Mechanistic basis of otolith formation during teleost inner ear development. *Dev. Cell* **20**, 271–278 (2011).
26. P. E. Gray, D. Sillence, A. Kakakios, Is Roifman syndrome an X-linked ciliopathy with humoral immunodeficiency? Evidence from 2 new cases. *Int. J. Immunogenet.* **38**, 501–505 (2011).
27. G. M. Abdel-Salam *et al.*, A homozygous mutation in *RNU4ATAC* as a cause of microcephalic osteodysplastic primordial dwarfism type I (MOPD I) with associated pigmentary disorder. *Am. J. Med. Genet. A* **155A**, 2885–2896 (2011).
28. S. Eisa-Beygi *et al.*, Characterization of endothelial cilia distribution during cerebral-vascular development in Zebrafish (Danio rerio). *Arterioscler. Thromb. Vasc. Biol.* **38**, 2806–2818 (2018).
29. S. Kallakuri *et al.*, Endothelial cilia are essential for developmental vascular integrity in zebrafish. *J. Am. Soc. Nephrol.* **26**, 864–875 (2015).
30. A. Buskin *et al.*, Disrupted alternative splicing for genes implicated in splicing and ciliogenesis causes PRPF31 retinitis pigmentosa. *Nat. Commun.* **9**, 4234 (2018).
31. C. B. Mellough *et al.*, An integrated transcriptional analysis of the developing human retina. *Development* **146**, dev169474 (2019).
32. M. R. Kraus *et al.*, Two mutations in human *BICC1* resulting in Wnt pathway hyperactivity associated with cystic renal dysplasia. *Hum. Mutat.* **33**, 86–90 (2012).
33. H. E. Shamseldin *et al.*, Mutations in *DDX59* implicate RNA helicase in the pathogenesis of orofaciodigital syndrome. *Am. J. Hum. Genet.* **93**, 555–560 (2013).
34. M. V. Akinyi, M. J. Frilander, At the intersection of major and minor spliceosomes: Crosstalk mechanisms and their impact on gene expression. *Front. Genet.* **12**, 700744 (2021).
35. M. Failler *et al.*, Mutations of *CEP83* cause infantile nephronophthisis and intellectual disability. *Am. J. Hum. Genet.* **94**, 905–914 (2014).
36. S. Thomas *et al.*, *TCTN3* mutations cause Mohr-Majewski syndrome. *Am. J. Hum. Genet.* **91**, 372–378 (2012).
37. A. Alexa, J. Rahnenfuhrer, T. Lengauer, Improved scoring of functional groups from gene expression data by decorrelating GO graph structure. *Bioinformatics* **22**, 1600–1607 (2006).
38. T. J. P. van Dam *et al.*, CiliaCarta: An integrated and validated compendium of ciliary genes. *PLoS One* **14**, e0216705 (2019).
39. O. Arnaiz, J. Cohen, A. M. Tassin, F. Koll, Remodeling Cildb, a popular database for cilia and links for ciliopathies. *Cilia* **3**, 9 (2014).
40. O. Arnaiz *et al.*, Cildb: A knowledgebase for centrosomes and cilia. *Database (Oxford)* **2009**, bap022 (2009).
41. C. B. Kimmel, W. W. Ballard, S. R. Kimmel, B. Ullmann, T. F. Schilling, Stages of embryonic development of the zebrafish. *Dev. Dyn.* **203**, 253–310 (1995).
42. B. Perner, C. Englert, F. Bollig, The Wilms tumor genes wt1a and wt1b control different steps during formation of the zebrafish pronephros. *Dev. Biol.* **309**, 87–96 (2007).
43. A. Borovina, S. Superina, D. Voskas, B. Ciruna, Vangl2 directs the posterior tilting and asymmetric localization of motile primary cilia. *Nat. Cell Biol.* **12**, 407–412 (2010).